

The influence of artificial aging on the microstructure and hardness of an Al–Zn–Mg–Zr alloy processed by equal-channel angular pressing

Jenő Gubicza, János L. Lábár, János Lendvai & Nguyen Q. Chinh

Journal of Materials Science

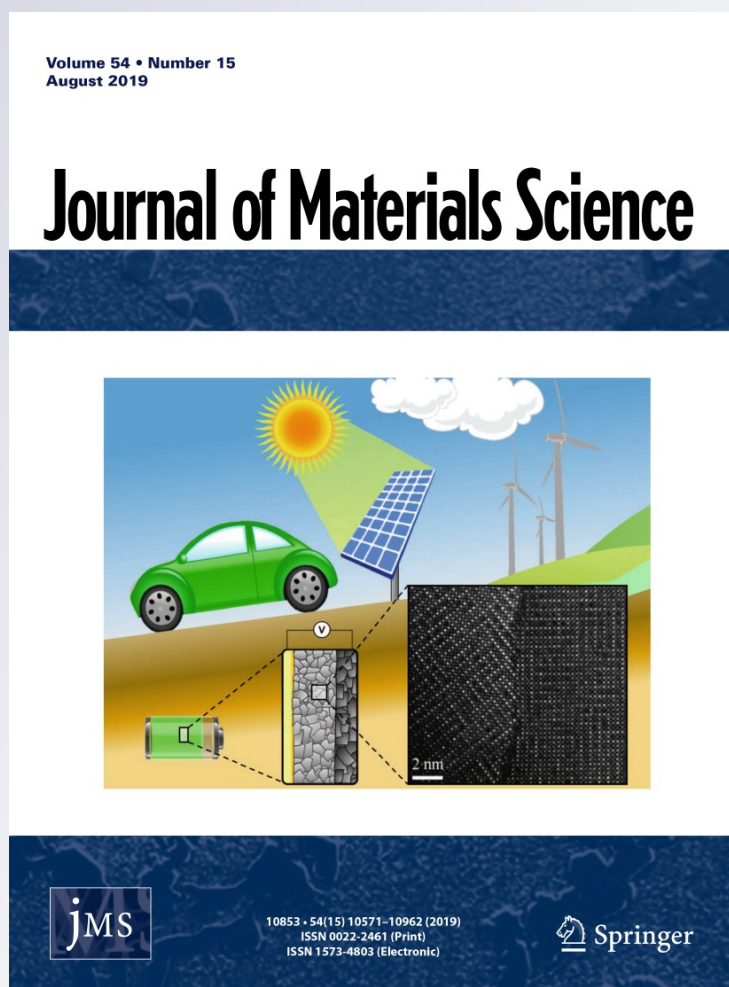
ISSN 0022-2461

Volume 54

Number 15

J Mater Sci (2019) 54:10918–10928

DOI 10.1007/s10853-019-03646-x



Your article is published under the Creative Commons Attribution license which allows users to read, copy, distribute and make derivative works, as long as the author of the original work is cited. You may self-archive this article on your own website, an institutional repository or funder's repository and make it publicly available immediately.



The influence of artificial aging on the microstructure and hardness of an Al–Zn–Mg–Zr alloy processed by equal-channel angular pressing

Jenő Gubicza^{1,*} , János L. Lábár^{1,2} , János Lendvai¹ , and Nguyen Q. Chinh¹

¹Department of Materials Physics, ELTE Eötvös Loránd University, P.O.B. 32, Budapest 1518, Hungary

²Institute for Technical Physics and Materials Science, Centre for Energy Research, Hungarian Academy of Sciences, Budapest, Hungary

Received: 6 February 2019

Accepted: 17 April 2019

Published online:
29 April 2019

© The Author(s) 2019

ABSTRACT

The effect of artificial aging on the microstructure and hardness of an ultrafine-grained (UFG) Al–4.8%Zn–1.2%Mg–0.14%Zr (wt%) alloy was studied. The UFG microstructure with an average grain size of about 260 nm was obtained by severe plastic deformation applying four passes of equal-channel angular pressing (ECAP) at room temperature. Then, artificial aging was performed on the ECAP-processed samples at 120 °C and 170 °C for 2 h. In the ECAP-processed sample Guinier–Preston (GP) zones, MgZn₂ precipitates and a high dislocation density were observed. After aging at 120 °C, coarse MgZn₂ precipitates were formed in the grain boundaries, leading to softening, while the dislocation density did not decrease. Annealing at 170 °C yielded a growth of the matrix grains to ~ 530 nm with a significant decrease in the dislocation density. In addition, GP zones disappeared and MgZn₂ precipitates were formed in both the grain interiors and the boundaries. This overaging of the precipitate structure and the decrease in the dislocation density resulted in a lower hardness than after annealing at 120 °C. It was found that the hardness reduction due to the change of the precipitate structure at 170 °C was higher than that caused by the decrease in the dislocation density.

Introduction

There is a large interest in age-hardenable Al–Zn–Mg alloys (7xxx series) due to their technological and practical importance, as these alloys can be treated to

have a preferable combination of ductility and strength, as well as reasonable weldability and corrosion resistance. If a supersaturated Al–Zn–Mg alloy is aged under different conditions, various metastable and stable precipitates may form [1–8]. Therefore, aging can be used for tailoring the

This work was dedicated to Prof. T. G. Langdon on the occasion of his 80th birthday.

Address correspondence to E-mail: jeno.gubicza@ttk.elte.hu

mechanical behavior of these alloys. Since the supersaturated state is thermodynamically unstable, the aging process may start at room temperature (RT) immediately after solution treatment and quenching. The decomposition of the supersaturated solid solution (SSSS) takes place by the formation of Guinier–Preston (GP) zones at RT. For higher aging temperatures (typically between 80 and 150 °C), metastable intermediate η' particles are formed directly from the SSSS and/or mediately from the GP zones. At higher temperatures, the formation of stable η precipitates with a composition of MgZn_2 is expected. It should be emphasized that significant strengthening can be achieved by the formation of GP zones and/or η' particles. For an effective application of aging on tailoring the mechanical properties of Al–Zn–Mg alloys, it is necessary to know the influence of the chemical composition and the history of the sample (e.g., pre-deformation) on the precipitation during aging.

Considering the promoting effect of dislocations on precipitation, a small amount of pre-strain is usually applied to the samples by conventional tension or compression in order to enhance the probability of the formation of metastable precipitates during subsequent natural aging [9]. In the last two decades, severe plastic deformation (SPD) by equal-channel angular pressing (ECAP) was applied to change the microstructure, thereby improving the mechanical properties (both strength and ductility) of supersaturated alloys [10–16]. This procedure imposes a large strain on the sample, causing a high dislocation density and also resulting in an ultrafine-grained (UFG) microstructure, thereby improving the strength of metallic materials. Although the microstructure obtained by ECAP has been extensively studied in the literature, the effect of artificial aging on the precipitation and the strength of SPD-processed supersaturated Al–Zn–Mg alloys have not been clarified so far.

In this paper, the effect of artificial aging on the microstructure and hardness of an UFG Al–4.8%Zn–1.2%Mg–0.14%Zr (wt%) alloy is studied. The UFG microstructure was obtained by four passes of ECAP at RT. Then, the ECAP-processed billets were aged at 120 °C and 170 °C for 2 h as these aging conditions are often applied on the homogenized undeformed counterparts of this alloy [4, 17]. The influence of aging on the grain size, dislocation density and precipitate structure was investigated for both

temperatures. The changes in the microstructure caused by aging were correlated with the hardness variation.

Materials and methods

Processing of the samples

An alloy with the composition of Al–4.8%Zn–1.2%Mg–0.14%Zr (wt%) was processed by casting. The addition of the small amount of Zr can ensure a fine-grained structure [18–21]. The as-cast material was homogenized in air at 470 °C for 8 h and then hot-extruded to a sheet of $10 \times 40 \text{ mm}^2$ cross section at 380 °C. The average grain size in the extruded material was about 10 μm . Cylindrical billets with 10 mm in diameter and 70 mm in length were fabricated from the extruded sheet, then subjected to solution heat treatment at 470 °C for 30 min and water-quenched in order to receive a supersaturated solid solution. The samples were processed by ECAP at RT for 4 passes within 10 min after quenching. The ECAP die had an internal channel angle of 90° and an outer arc of curvature at the intersection of the two parts of the channel of 20°, giving an imposed strain of about 1 on each separate pass [22]. The samples were processed following route B_c in which the billets are rotated in the same sense around their longitudinal axes by 90° after each pass [23]. The ECAP-processed samples were stored at RT for a long period (about 1 year) and then artificially aged at 120 °C or 170 °C for 2 h in an oil-bath.

Microstructure characterization techniques

The phase composition of the ECAP-processed and the aged specimens were studied by X-ray diffraction (XRD) using a Philips Xpert powder diffractometer with $\text{CuK}\alpha$ radiation (wavelength: $\lambda = 0.15418 \text{ nm}$).

The microstructure was characterized by X-ray line profile analysis (XLPA) using a high-resolution diffractometer (type: MultiMax-9, manufacturer: Rigaku, Japan) with $\text{CuK}\alpha_1$ radiation (wavelength: $\lambda = 0.15406 \text{ nm}$). The diffraction patterns were then evaluated by the Convolutional Multiple Whole Profile (CMWP) fitting procedure [24]. In the CMWP method, the experimental diffraction pattern is fitted by the sum of a background spline and the convolution of the instrumental pattern and the theoretical

line profiles related to the diffraction domain size and the lattice strain caused by dislocations. The instrumental pattern was measured on a LaB₆ line profile standard material. The area-weighted mean diffraction domain size ($\langle x \rangle_{\text{area}}$) and the average dislocation density (ρ) were determined from the line profile fitting. The area-weighted mean diffraction domain size was calculated as $\langle x \rangle_{\text{area}} = m \cdot \exp(2.5 \sigma^2)$, where m is the median and σ^2 is the log-normal variance of the diffraction domain size distribution.

The size and morphology of the matrix grains and the precipitates were characterized by transmission electron microscopy (TEM). Thin TEM lamellae were prepared from pieces of the bulk samples by Ar-ion milling with special care taken to avoid heating (and possible transformation) of the samples during preparation. Firstly, the samples were glued by using a special glue at 100 °C for not more than 1 min to a Cu stub for mechanical grinding and polishing. In the second step, ion-beam thinning of the 50- μm -thick lamella was started at 7 keV using 2 mA ion current. Finally, the just perforated lamella was cleaned at 3 keV and later at 1 keV from both sides to remove damaged layers from its surfaces.

The TEM, high-resolution TEM (HRTEM) and energy-disperse X-ray spectroscopy (EDS) examinations were performed in a Titan Themis G2 200 scanning TEM (STEM) equipped with a four-segment Super-X EDS detector. The corrector for the spherical aberration (C_s) was applied at the imaging part, while no probe correction was present. Image resolution limit is 0.08 nm in phase-contrast HRTEM mode, while resolution is 0.16 nm in STEM Z-contrast imaging mode (recorded with a Fischione high-angle annular dark-field (HAADF) detector). HRTEM images were recorded at 200 keV with a 4 k \times 4 k CETA 16 CMOS camera controlled by VELOX software. EDS data were recorded (together with the HAADF signal) in spectrum image (SI) mode, where individual X-ray count data can later be post-processed pixel-by-pixel and elemental intensities (and quantified elemental concentrations) can be obtained from any post-selected regions. In that way, distribution of concentrations can be visualized along any lines or over any area and the values can also be obtained in a tabulated form.

Hardness testing

The microhardness of the samples was measured at RT using a ZwickRoell ZH μ hardness tester with a Vickers indenter, an applied load of 500 g and a dwell time of 10 s. The average hardness values were obtained from at least 10 individual measurements.

Experimental results

XRD study of the phase composition and the microstructure characteristics

Figure 1 shows XRD patterns obtained on the ECAP-processed and the aged specimens. In order to a better visibility of the peaks of the precipitates, only a part of the diffractograms (for the diffraction angle range $2\theta = 34\text{--}48^\circ$) is shown with logarithmic intensity scale. It is noted that the entire 2θ range of the measured patterns spreads from 15° to 140° . Figure 1 reveals that in addition to the peaks of the face-centered cubic (fcc) Al matrix, X-ray reflections of a secondary phase also appeared on the diffractogram taken on the ECAP-processed sample. This phase was identified as η -MgZn₂ with hexagonal close packed (hcp) structure and lattice constants $a = 0.5223$ nm and $c = 0.8568$ nm (PDF card number: 34-0457). Peaks of η' precipitates were not detected (PDF card number: 31-0024). The ratio of the sums of the peak intensities (the areas under the peaks after background subtraction) of the MgZn₂ precipitates and the matrix is shown in Table 1. This ratio is

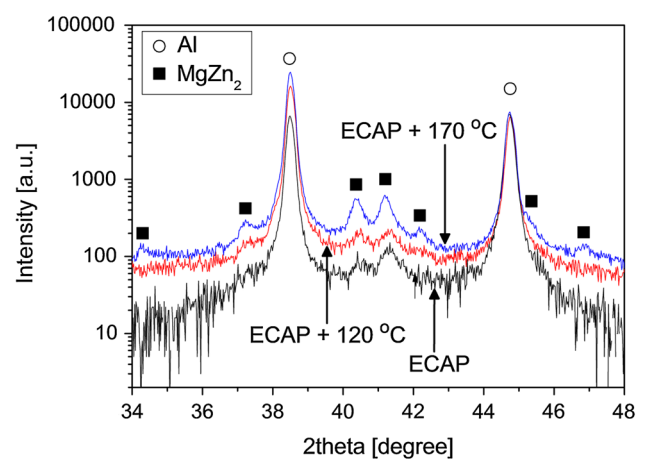


Figure 1 A part of the XRD patterns measured on the ECAP-processed sample and the specimens aged at 120 and 170 °C for 2 h.

0.9 ± 0.2% for the specimen processed by four passes of ECAP. It is noted that this value is not equivalent to the volume ratio of the two phases as the unit volumes of the crystalline phases with different structures and chemical compositions usually scatter X-rays with different intensities. Nevertheless, the change of the fraction of precipitates during aging can be monitored using this quantity. Figure 1 shows that the peaks of the MgZn₂ phase also appeared in the diffractograms obtained for the aged samples. The intensity fraction of this phase remained unchanged after annealing at 120 °C (0.9 ± 0.2%), but it increased after annealing at 170 °C to 6.8 ± 0.9% after aging at 170 °C.

As an example of the XLPAs evaluation, Fig. 2 shows the measured XRD pattern and the fitted diffractogram obtained by the CMWP method for the ECAP specimen aged at 170 °C. The average diffraction domain size and dislocation density determined by the CMWP fitting procedure for the three studied samples are listed in Table 1. After ECAP processing, the diffraction domain size was about 100 nm which remained unchanged during aging at both temperatures. The dislocation density in the ECAP-processed specimen was ~ 5 × 10¹⁴ m⁻². This value did not change significantly during annealing at 120 °C. At the same time, aging at 170 °C yielded a decrease in the dislocation density to ~ 3.3 × 10¹⁴ m⁻².

Investigation of the microstructure by TEM

Figure 3a shows a TEM image on the microstructure of the ECAP-processed sample. The average grain size of the matrix was about 260 ± 30 nm as determined by TEM (also listed in Table 1). The average grain size was obtained from about twenty grains for

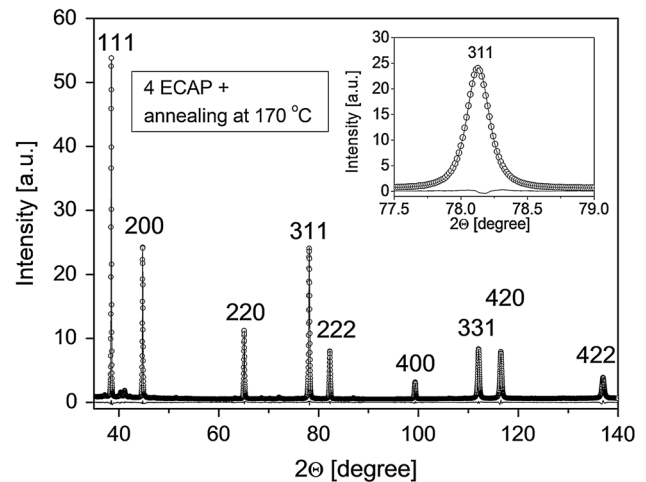


Figure 2 The measured XRD pattern (open circles) and the diffractogram fitted by the CMWP method (solid line) for the ECAP specimen aged at 170 °C. The difference between the measured and fitted data can be seen at the bottom of the figure. In order to a better visibility of the fitting quality, the inset shows the magnified reflection 311.

each sample. It should be noted that in the present samples the grain size obtained by TEM was about 3–5 times larger than the diffraction domain size evaluated by XLPAs. This difference is usual in SPD-processed materials as the diffraction domains correspond to subgrains and/or dislocation cells inside the grains [25]. The ECAP-processed specimen contains precipitates, mainly in the interiors of the grains, as illustrated by the bright areas in Fig. 3a. Some larger particles can be found at the grain boundaries. Figure 3b shows that inside the grains there are smaller precipitates with a size of ~ 2 nm and larger particles with a diameter of about 10–20 nm. The corresponding EDS elemental maps for Al, Zn, Mg and Zr are shown in Fig. 3c–f, respectively. The white and black arrows in Fig. 3b

Table 1 The XRD intensity fraction of MgZn₂ precipitates as well as the diffraction domain size and the dislocation density in the Al matrix as determined by XLPAs. The average grain size values in the matrix determined by TEM are also shown

Samples	Intensity fraction of MgZn ₂ (%)	Diffraction domain size in the matrix (nm)	Dislocation density in the matrix (10 ¹⁴ m ⁻²)	Grain size in the matrix from TEM (nm)
4 ECAP at RT	0.9 ± 0.2	92 ± 10	4.8 ± 0.5	260 ± 30
4 ECAP + aged at 120 °C	0.9 ± 0.2	105 ± 11	5.0 ± 0.5	310 ± 50
4 ECAP + aged at 170 °C	6.8 ± 0.9	111 ± 12	3.3 ± 0.4	530 ± 50

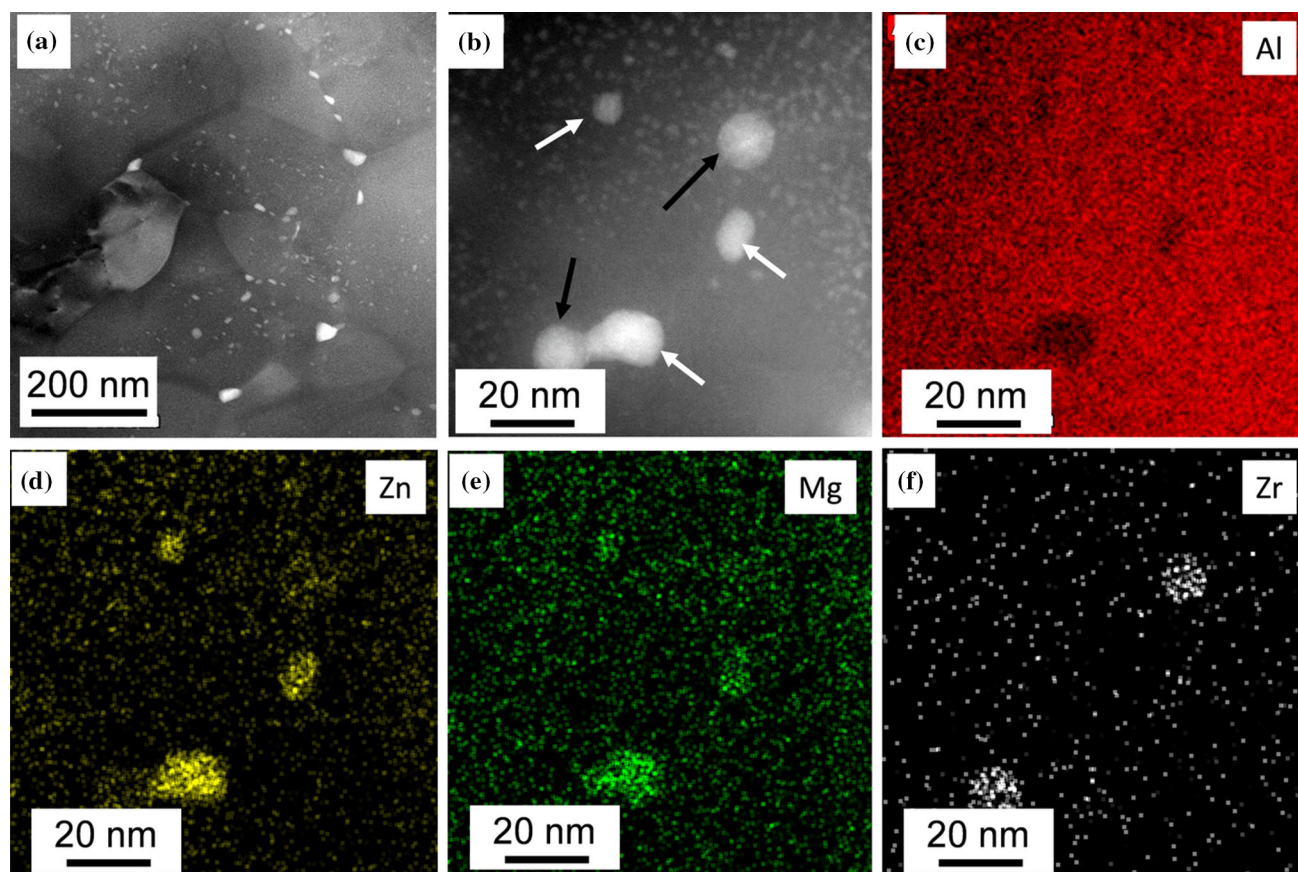


Figure 3 **a** HAADF STEM image illustrating the microstructure of the ECAP-processed sample. **b** HAADF STEM image with a higher magnification showing precipitates. **c–f** EDS elemental

maps for Al, Zn, Mg and Zr obtained on the area shown in **b**. The white and black arrows in **b** indicate Mg/Zn- and Zr-rich precipitates, respectively. The Mg/Zn-rich precipitates are depleted of Al as shown in Fig. 3c. Therefore, these particles are most probably the MgZn_2 precipitates identified by XRD (see Fig. 1). The size of these particles is between 10 and 20 nm in good accordance with the apparent diffraction domain size value estimated from the breadths of the XRD peaks of this phase (~ 20 nm). The size of the Zr-rich precipitates was 10–15 nm as shown in Fig. 3b. The XRD peaks of this phase were not revealed in the diffractograms since the fraction of the Zr-rich phase must be low due to the small overall concentration of Zr (0.14 wt%). Similar Zr-rich precipitates were identified formerly as Al_3Zr particles [26]. Previous studies (e.g., [20, 21]) have shown that the coherent Al_3Zr precipitates pin effectively the grain boundaries formed in SPD processing, thereby preventing grain coarsening during annealing. In addition to MgZn_2 and Zr-rich particles, many small precipitates with the size of about

maps for Al, Zn, Mg and Zr obtained on the area shown in **b**. The white and black arrows in **b** indicate Mg/Zn- and Zr-rich precipitates, respectively.

2 nm appeared inside the matrix grains (see Fig. 3b). Most probably, these particles are GP zones.

Figure 4a shows the microstructure of the ECAP-processed sample aged at 120 °C for 2 h. The grain size determined from the TEM images was 310 ± 50 nm (see also Table 1) which does not differ significantly from the value obtained immediately after ECAP (260 ± 30 nm). Figure 4b also reveals that the grain boundaries are decorated with particles having size between 10 and 30 nm. The elemental maps in Fig. 4c–f show that these precipitates are enriched with Zn and Mg. The chemical analysis and the XRD results (see Fig. 1) suggest that these particles in the grain boundaries are η - MgZn_2 precipitates. It is noted that similar particles also exist in the grain interiors but the larger ones can be found in the grain boundaries. In addition to MgZn_2 precipitates, the grains also contain GP zones with the size of about 2 nm. It must also be noted that in the vicinity of the grain boundaries the matrix was depleted of

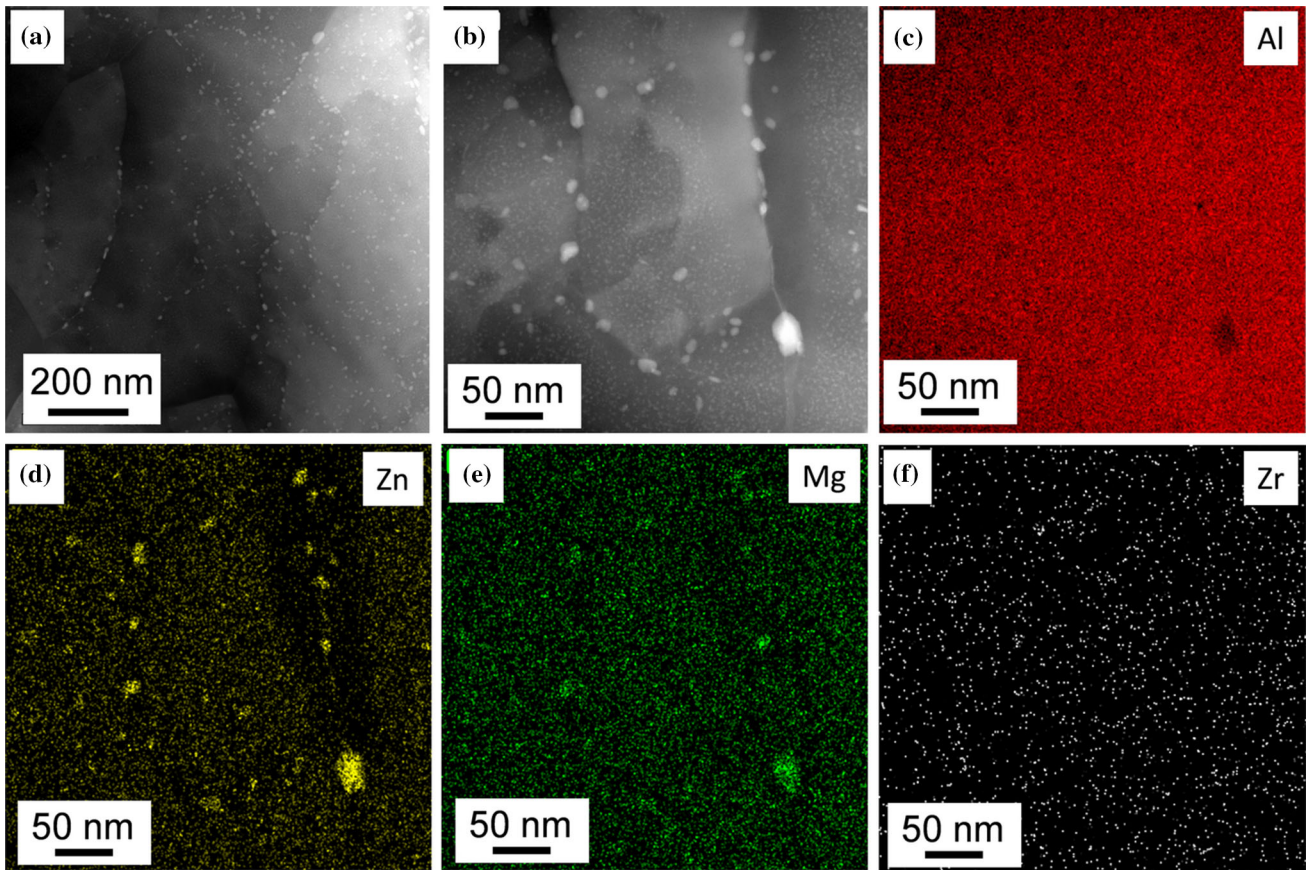


Figure 4 a HAADF STEM image illustrating the microstructure of the specimen processed by ECAP and then aged at 120 °C for 2 h. b HAADF STEM image with a higher magnification showing

GP zones as well as Mg and Zn atoms (e.g., see the area around the approximately vertical grain boundary at the right side of Fig. 4b, d, e).

During aging at 170 °C, the grain size increased to 530 ± 50 nm as determined by TEM (see Table 1). As an example, Fig. 5a shows a TEM image which also reveals that both the grain boundaries and the grain interiors contain large (10–100 nm) precipitates. In Fig. 5b, the image with a higher magnification shows particles inside a grain with sizes between 5 and 30 nm. The elemental maps in Fig. 5c–f reveal that these particles are Zn- and Mg-rich precipitates. Considering the result of the XRD phase analysis (see Fig. 1), these precipitates are identified as η -MgZn₂ particles. The morphology of the large Zn/Mg-rich precipitates in the left bottom corner of Fig. 5b suggests that these particles are disks with a hexagonal shape, i.e., the morphology at some extent reflects their hcp crystal structure. GP zones were not observed in the sample aged at 170 °C.

precipitates. c–f EDS elemental maps for Al, Zn, Mg and Zr obtained on the area shown in b.

Hardness of the ECAP-processed and the aged specimens

The hardness of the ECAP-processed specimen was 1470 ± 40 MPa which decreased significantly to 1230 ± 40 MPa due to aging at 120 °C for 2 h. The annealing at the higher temperature of 170 °C resulted in a considerably lower hardness with the value of 1100 ± 30 MPa. The reasons of the softening will be discussed in the next section.

Discussion

The present study revealed that the microstructure of the matrix in the ECAP-processed Al–4.8%Zn–1.2%Mg–0.14%Zr (wt%) alloy exhibited a good stability during aging at 120 and 170 °C for 2 h. Indeed, the grain size and the dislocation density remained practically unchanged during annealing at 120 °C

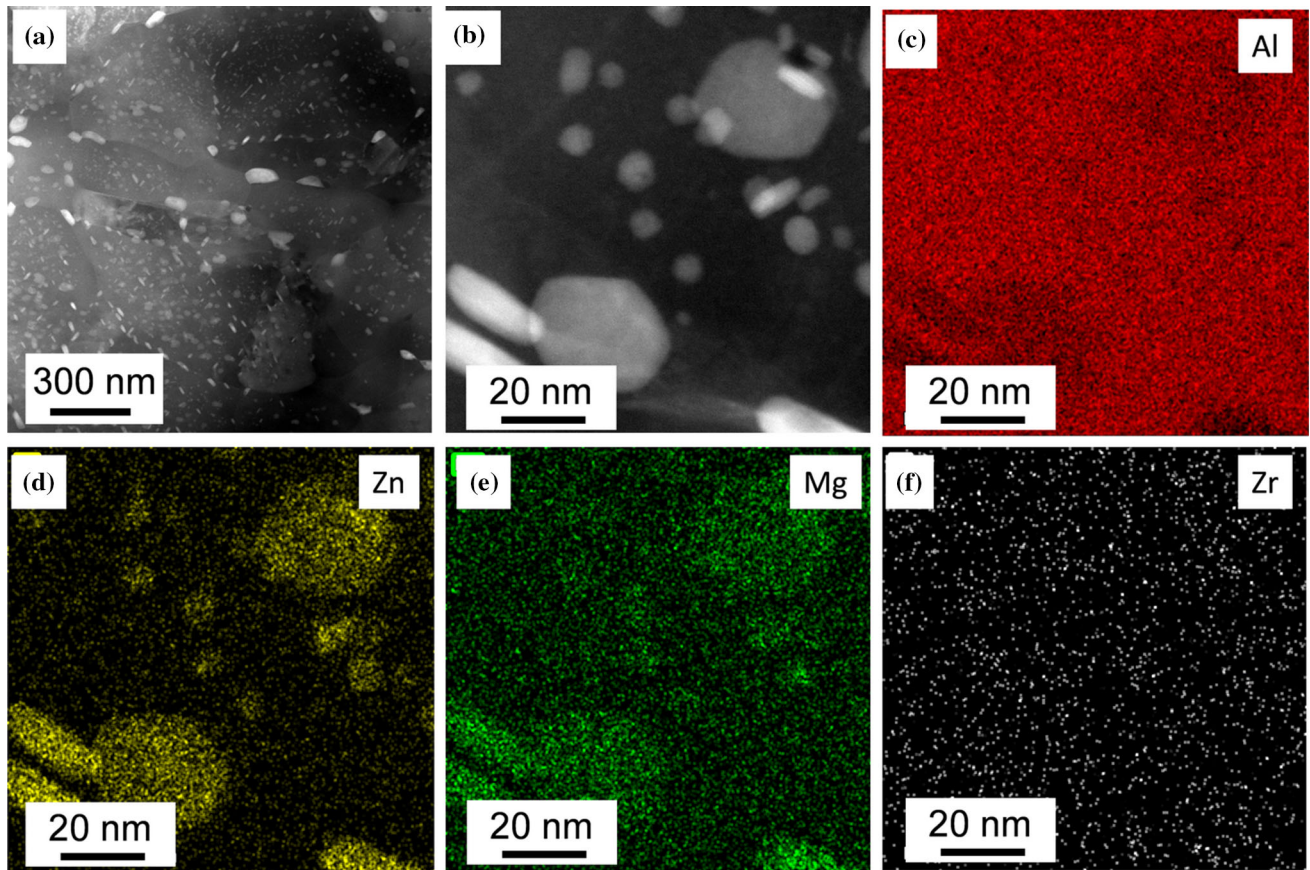


Figure 5 **a** HAADF STEM image illustrating the microstructure of the specimen processed by ECAP and then aged at 170 °C for 2 h. **b** HAADF STEM image with a higher magnification showing

precipitates. **c–f** EDS elemental maps for Al, Zn, Mg and Zr obtained on the area shown in **b**.

and the dislocation density decreased only moderately at 170 °C. At this temperature, there was a significant grain growth from 260 ± 30 to 530 ± 50 nm; nevertheless, the grain size remained in the UFG regime. The good thermal stability of the ECAP-processed alloy can be attributed to the hindering effect of precipitates (GP zones and MgZn_2 particles) on movement of lattice defects (dislocations and grain boundaries), thereby retarding dislocation annihilation and grain growth. This effect operates even if ECAP processing is performed on supersaturated solid solutions since SPD promotes precipitation in dispersion-strengthened alloys [27]. Indeed, in an Al–4.8%Zn–1.2%Mg–0.14%Zr alloy quenched to RT after annealing at 470 °C for 30 min and stored at RT for 1 year only GP zones and a few Zr-rich particles were observed as revealed by XRD (not shown here) and TEM (see Fig. 6). At the same time, in the alloy processed by four passes of ECAP after quenching and then stored at RT for 1 year a

considerable amount of MgZn_2 particles was formed (see Fig. 3).

Aging of the ECAP-processed sample at 120 and 170 °C for 2 h resulted in a change of the precipitate structure. At 120 °C considerable change in the fraction of MgZn_2 phase was not observed by XRD, but TEM revealed coarsening of these precipitates. This process was most significant at the grain boundaries which can be explained by the accelerated diffusion along these boundaries in the UFG microstructure. As a result, an inhomogeneous spatial distribution of precipitates was observed in the sample annealed at 120 °C for 2 h. At the higher aging temperature of 170 °C, the diffusion rate was high enough even inside the grains for resulting in a more homogeneous precipitate structure where relatively large MgZn_2 particles (~ 30 nm) can be found in both the grain interiors and the boundaries.

The hardness of the ECAP-processed alloy decreased from 1470 ± 40 to 1230 ± 40 MPa and

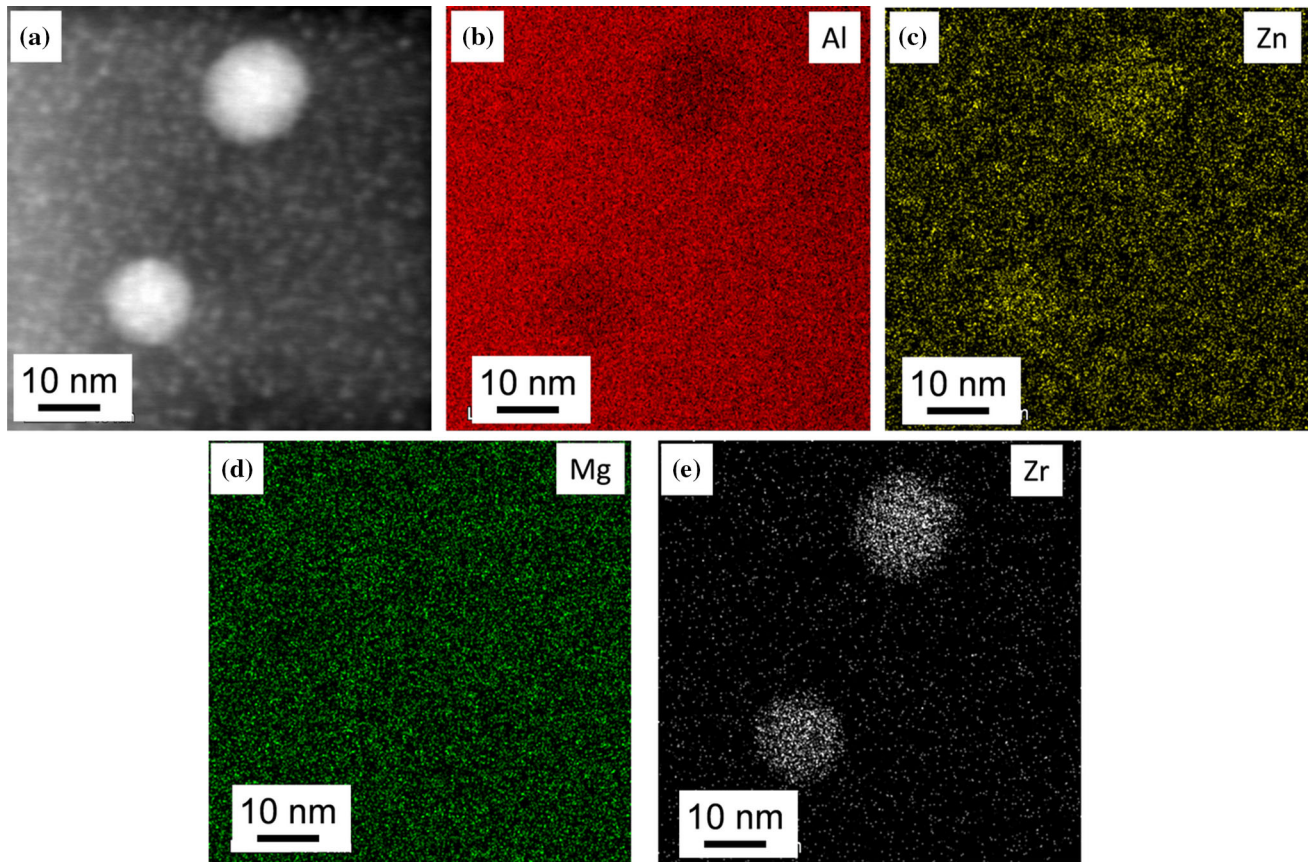


Figure 6 **a** HAADF STEM image showing precipitates in a sample quenched to RT after annealing at 470 °C for 30 min and stored at RT for 1 year. **b–e** EDS elemental maps for Al, Zn, Mg and Zr obtained on the area shown in **a**.

1100 ± 30 MPa, respectively, after aging at 120 and 170 °C for 2 h. For the lower aging temperature, the TEM results have shown a slight change in the matrix microstructure, indicating the dissolution of a part of GP zones. The hardness reduction in this sample should be attributed to the change in GP zone- and/or η' structure, as well as to the coarsening of MgZn₂ precipitates. The growth of η particles with an unchanged volume fraction usually results in softening since in this case dislocations overcome the incoherent precipitates with Orowan mechanism [3]. At the same time, during aging at 170 °C in addition to the significant change of the precipitate structure, the reduction of the dislocation density and grain growth also occurred, and all of these processes cause softening. Therefore, in the following the contributions of these processes to the hardness reduction will be estimated.

The hardness caused by dislocation strengthening (HV_{disl}) can be expressed by the Taylor formula as:

$$HV_{\text{disl}} \approx 3\alpha M^T G b \rho^{1/2}, \quad (1)$$

where α is a constant describing the dislocation strengthening (about 0.32 for Al [28]), G is the shear modulus (~ 26 GPa for Al), b is the magnitude of the Burgers vector (~ 0.287 nm for Al), and M^T is the Taylor factor. The alloys used in this investigation did not exhibit a strong texture and therefore M^T was taken as 3.06. The factor of three on the right-hand side of Eq. (1) represents the ratio of the hardness and the yield strength contributions of dislocations [29]. It should be noted that one-third of the hardness gives the flow stress at the plastic strain of 8% rather than the yield strength. However, for SPD-processed metallic materials the yield strength can be estimated as one-third of the hardness due to the low strain hardening. The values of HV_{disl} calculated from Eq. (1) are listed in Table 2. For the ECAP-processed sample, the contribution of dislocations to hardness was 480 ± 60 MPa which did not change during annealing at 120 °C. At the same time, aging at 170 °C resulted in a reduction of HV_{disl} to

400 ± 50 MPa. The hardness caused by the precipitates (HV_{precip}) was calculated as the difference between the total measured hardness (HV_{total}) and the sum of the contributions of dislocations and lattice friction (HV_0):

$$HV_{\text{precip}} = HV_{\text{total}} - (HV_0 + HV_{\text{disl}}). \quad (2)$$

The threshold hardness HV_0 was estimated as three times the friction stress for Al ($HV_0 = 60 \pm 10$ MPa [28]). It is noted that grain boundary strengthening was not considered as a separate Hall–Petch term in Eq. (2). Former investigations (e.g., [28]) showed that Eq. (1) is able to incorporate both grain size and dislocation hardening effects for fcc metallic materials processed by SPD. This can be explained by the fact that in SPD-processed materials many dislocations are accumulated at grain boundaries. Therefore, when a dislocation glides in the vicinity of a grain boundary it interacts with the grain boundary dislocations and not directly with the grain boundary.

The values of HV_{precip} obtained from Eq. (2) are also listed in Table 2. For the ECAP-processed specimen, the contribution of precipitates to the hardness is 930 ± 110 MPa which is much larger than that for dislocations (480 ± 60 MPa). During annealing at 120°C , HV_{precip} decreased to 690 ± 110 MPa, i.e., it was still higher than the hardness caused by dislocation strengthening (480 ± 60 MPa). Aging at 170°C yielded a decrease in both HV_{disl} and HV_{precip} , but the reduction of the contribution of precipitates was higher both relatively and absolutely compared to that of dislocations. Namely, the contributions of dislocations and precipitates to the decrease in the hardness are ~ 80 and ~ 290 MPa, respectively. Thus, the softening during aging at both temperatures of 120 and 170°C was caused mainly by the change of the precipitate structure, especially by the disappearance of GP zones formed during SPD.

Conclusions

The microstructure and the hardness of an UFG Al–Zn–Mg–Zr alloy artificially aged at 120 and 170°C for 2 h were studied. The UFG microstructure was obtained by four passes of ECAP at RT. The following conclusions were drawn from the experimental results:

1. ECAP resulted in an UFG microstructure with an average grain size of ~ 260 nm and a high dislocation density of about $5 \times 10^{14} \text{ m}^{-2}$. ECAP promoted precipitation since after four passes MgZn_2 precipitates with the size of about 10 nm were formed while the quenched and naturally aged sample contained mainly GP zones with the average diameter of ~ 2 nm.
2. The artificial aging of the ECAP-processed sample at 120°C for 2 h yielded a decrease in the hardness from 1470 ± 40 to 1230 ± 40 MPa due to a partial dissolution of GP zones and the coarsening of MgZn_2 precipitates, especially in the vicinity of grain boundaries. The evolution of the heterogeneous precipitate structure can be explained by the elevated rate of diffusion along the grain boundaries. At the same time, significant grain growth and a decrease in the dislocation density were not observed, i.e., the softening can be attributed solely to the change of the precipitate structure.
3. Annealing at 170°C for 2 h resulted in a considerable decrease in the dislocation density to $\sim 3.3 \times 10^{14} \text{ m}^{-2}$, a grain growth in the matrix to about 530 nm and a large increase in the amount of MgZn_2 precipitates. GP zones were not observed in this state of the material. The changes in the microstructure yielded a lower hardness for the sample aged at 170°C (1100 ± 30 MPa) than that after annealing at 120°C (1230 ± 40 MPa).
4. For the ECAP-processed specimen, a significant amount (more than 60%) of the hardness can be attributed to the strengthening effect of precipitates. This remained valid also for the samples

Table 2 The total measured microhardness (HV_{total}) and the calculated contributions of the lattice friction (HV_0), dislocations (HV_{disl}) and precipitates (HV_{precip})

Samples	HV_{total} (MPa)	HV_0 (MPa)	HV_{disl} (MPa)	HV_{precip} (MPa)
4 ECAP at RT	1470 ± 40	60 ± 10	480 ± 60	930 ± 110
4 ECAP + aged at 120°C	1230 ± 40	60 ± 10	480 ± 60	690 ± 110
4 ECAP + aged at 170°C	1100 ± 30	60 ± 10	400 ± 50	640 ± 90

aged after ECAP. The reduction of hardness during annealing was caused mainly by the change of the precipitate structure. For instance, during aging at 170 °C the contributions of dislocations and precipitates to the decrease in the hardness were ~ 80 and ~ 290 MPa, respectively.

Acknowledgements

Open access funding provided by Eötvös Loránd University (ELTE). This research was supported by the Hungarian–Russian bilateral Research Program (TÉT) No. 2017-2.3.4-TÉT-RU-2017-00005. This work was financed partly by the Ministry of Human Capacities of Hungary within the ELTE University Excellence program (1783-3/2018/FEKUTSRAT). This work was also supported by the Project VEKOP-2.3.3-15-2016-00002 of the European Structural and Investment Funds.

Compliance with ethical standards

Conflict of interest The authors declare that there is no conflict of interest.

Open Access This article is distributed under the terms of the Creative Commons Attribution 4.0 International License (<http://creativecommons.org/licenses/by/4.0/>), which permits unrestricted use, distribution, and reproduction in any medium, provided you give appropriate credit to the original author(s) and the source, provide a link to the Creative Commons license, and indicate if changes were made.

References

- [1] Mondolfo LF (1971) Structure of the aluminium: magnesium: zinc alloys. *Int Metall Rev* 153:95–124
- [2] Polmear IJ (1995) *Light alloys-metallurgy of the light metals*, 3rd edn. Arnold, London
- [3] Lendvai J (1996) Precipitation and strengthening in aluminium alloys. *Mater Sci Forum* 217–222:43–56
- [4] Löffler H, Kovács I, Lendvai J (1983) Decomposition processes in Al–Zn–Mg alloys. *J Mater Sci* 18:2215–2240. <https://doi.org/10.1007/BF00541825>
- [5] Liddicoat PV, Liao XZ, Zhao Y, Zhu Y, Murashkin MY, Lavernia EJ, Valiev RZ, Ringer SP (2010) Nanostructural hierarchy increases the strength of aluminium alloys. *Nat Commun* 1:63. <https://doi.org/10.1038/ncomms1062>
- [6] Watanabe K, Matsuda K, Ikeno S, Yoshida T, Murakami S (2015) TEM observation of precipitate structures in Al–Zn–Mg alloys with addition of Cu/Ag. *Metall Mater* 60:977–979
- [7] Wu C, Ma K, Zhang D, Wu J, Luo G, Zhang J, Chen F, Shen Q, Zhang L, Lavernia EJ (2017) Precipitation phenomena in Al–Zn–Mg alloy matrix composites reinforced with B₄C particles. *Sci Rep* 7:9589. <https://doi.org/10.1038/s41598-017-10291-4>
- [8] Bobruk E, Murashkin MY, Kazykhanov VU, Valiev RZ (2018) Superplastic behavior at lower temperatures of high strength ultrafine-grained Al alloy 7475. *Adv Eng Mater* 21:1800094. <https://doi.org/10.1002/adem.201800094>
- [9] Wang D, Ma ZY (2009) Effect of pre-strain on microstructure and stress corrosion cracking of over-aged 7050 aluminum alloy. *J Alloys Compd* 469:445–450
- [10] Zhao YH, Liao XZ, Jin Z, Valiev RZ, Zhu YT (2004) Microstructures and mechanical properties of ultrafine grained 7075 Al alloy processed by ECAP and their evolutions during annealing. *Acta Mater* 52:4589–4599
- [11] Xu C, Furukawa M, Horita Z, Langdon TG (2005) Influence of ECAP on precipitate distributions in a spray-cast aluminum alloy. *Acta Mater* 53:749–758
- [12] Xu C, Furukawa M, Horita Z, Langdon TG (2003) Using ECAP to achieve grain refinement, precipitate fragmentation and high strain rate superplasticity in a spray-cast aluminum alloy. *Acta Mater* 51:6139–6149
- [13] Gubicza J, Schiller I, Chinh NQ, Illy J, Horita Z, Langdon TG (2007) The effect of severe plastic deformation on precipitation in supersaturated Al–Zn–Mg alloys. *Mater Sci Eng A* 460–461:77–85
- [14] Samaee M, Najafi S, Eivani AR, Jafarian HR, Zhou J (2016) Simultaneous improvements of the strength and ductility of fine-grained AA6063 alloy with increasing number of ECAP passes. *Mater Sci Eng A* 669:350–357
- [15] Ashrafizadeh SM, Eivani AR, Jafarian HR, Zhou J (2017) Improvement of mechanical properties of AA6063 aluminum alloy after equal channel angular pressing by applying a two-stage solution treatment. *Mater Sci Eng A* 687:54–62
- [16] Duan ZC, Chinh NQ, Xu Ch, Langdon TG (2010) Developing processing routes for the equal-channel angular pressing of age-hardenable aluminum alloys. *Metall Mater Trans* 41A:802–809
- [17] Chinh NQ, Lendvai J, Ping DH, Hono K (2004) The effect of Cu on mechanical and precipitation properties of Al–Zn–Mg alloys. *J Alloys Compd* 378:52–60
- [18] Dorward RC, Beerntsen DJ (1995) Grain structure and quench-rate effects on strength and toughness of AA7050

- Al–Zn–Mg–Cu–Zr alloy plate. *Metall Trans A* 26:2481–2484
- [19] Chinh NQ, Juhász A, Tasnádi P, Lendvai J, Kovács I (1993) Effect of copper and zirconium upon the high temperature mechanical properties of AlMgZn alloys. *Phys Stat Sol (a)* 138:175–184
- [20] Eivani AR, Zhou J, Duszczyc J (2012) A new approach to incorporating the effect of nano-sized dispersoids on recrystallization inhibition into Monte carlo simulation. *Comput Mater Sci* 54:370–377
- [21] Buranova Y, Kulitskiy Peterlechner M, Mogucheva A, Kaibyshev R, Divinski SV, Wilde G (2017) Al₃(Sc, Zr)-based precipitates in Al–Mg alloy: effect of severe deformation. *Acta Mater* 124:210–224
- [22] Iwahashi Y, Wang J, Horita Z, Nemoto M, Langdon TG (1996) Principle of equal-channel angular pressing for the processing of ultra-fine grained materials. *Scr Mater* 35:143–146
- [23] Furukawa M, Iwahashi Y, Horita Z, Nemoto M, Langdon TG (1998) The shearing characteristics associated with equal-channel angular pressing. *Mater Sci Eng A* 257:328–332
- [24] Ribárik G, Gubicza J, Ungár T (2004) Correlation between strength and microstructure of ball-milled Al–Mg alloys determined by X-ray diffraction. *Mater Sci Eng A* 387–389:343–347
- [25] Ungár T, Tichy G, Gubicza J, Hellmig RJ (2005) Correlation between subgrains and coherently scattering domains. *Powder Diffr* 20:366–375
- [26] Priya P, Krane MJM, Johnson DR (2016) Precipitation of Al₃Zr dispersoids during homogenization of Al–Zn–Cu–Mg–Zr alloys. In: Williams E (ed) *Light metals 2016*. Springer, Cham, pp 213–218
- [27] Gubicza J, Schiller I, Chinh NQ, Illy J, Horita Z, Langdon TG (2007) The effect of severe plastic deformation on precipitation in supersaturated Al–Zn–Mg alloys. *Mater Sci Eng A* 460–461:77–85
- [28] Gubicza J, Chinh NQ, Lábár JL, Hegedűs Z, Xu C, Langdon TG (2008) Microstructure and yield strength of severely deformed silver. *Scr Mater* 58:775–778
- [29] Tabor D (1951) *Hardness of metals*. Clarendon Press, Oxford

Publisher's Note Springer Nature remains neutral with regard to jurisdictional claims in published maps and institutional affiliations.